

Picking-up Local GRB Candidates Based on Their Host Galaxies

J. WANG,^{1,2,3} Y. XU,¹ L. J. CHEN,² C. WU,^{1,4} L. P. XIN,¹ E. W. LIANG,^{2,3} AND J. Y. WEI^{1,4}

¹*Key Laboratory of Space Astronomy and Technology, National Astronomical Observatories, Chinese Academy of Sciences, Beijing 100101, People's Republic of China*

²*Guangxi Key Laboratory for Relativistic Astrophysics, School of Physical Science and Technology, Guangxi University, Nanning 530004, People's Republic of China*

³*GXU-NAOC Center for Astrophysics and Space Sciences, Nanning, 530004, People's Republic of China*

⁴*School of Astronomy and Space Science, University of Chinese Academy of Sciences, Beijing, People's Republic of China*

ABSTRACT

Rapid identification of candidates of high-value gamma-ray bursts (GRBs), including both high- z and local events, is crucial for outlining subsequent observational strategy. In this paper, we present a model that enables an on-duty astronomer to rapidly identify candidates of local GRBs prior to spectroscopy, provided that these events have been localized at an arcseconds precision. After taking into account the mass distribution of the host galaxies of GRBs, the model calculates the two-dimensional cross-match probabilities between a localized GRB and its surrounding nearby galaxies, and then returns the best match with the highest probability. The model is evaluated not only by the observed GRB sample with redshifts up to $z = 4$, but also through the simulated GRB samples. By using the recently published GLADE+ galaxies catalog with a completeness of 95% up to 500Mpc, along with the NED-LVS catalog, the Precision and Recall of the model are determined to be 0.23-0.33 and 0.75, respectively, at the best performance. A dedicated web service, which will be integrated into the SVOM Science User Support System, has been developed to deploy the model.

Keywords: gamma-ray burst: general — methods: statistical — galaxies: distances and redshifts

1. INTRODUCTION

Gamma-ray bursts (GRBs) are the most powerful explosions occurring in the universe (e.g., Hjorth & Bloom 2012). There is compelling observational evidence supporting that the GRBs originate from either the core-collapse of young massive stars ($\geq 25M_{\odot}$; e.g., Woosley & Bloom 2006 and references therein) or the merger of neutron star binaries (e.g., Berger 2014 and references therein).

Due to these widely accepted origins, GRBs are believed to occur from local to distant universe up to a redshift of ~ 20 (e.g., Lamb & Reichart 2000). Although high- z GRBs are fascinating in the exploration of the early universe (e.g., Tagliaferri et al. 2005; Greiner et al. 2009; Tanvir et al. 2009, 2018; Melandri et al. 2015; Cucchiara et al. 2011), the local, and usually bright, GRBs are still important because they allow us to explore the nature of the progenitor and environment of

a GRB comprehensively through either high-quality afterglow spectra or well resolved host galaxy.

In fact, the aforementioned collapse and merger scenarios are confirmed by the detection of a supernova (SN) or a kilonova associated with a GRB, respectively. On the one hand, mainly because of the faintness of the associated SNe, there are, so far, only 30 spectroscopically confirmed GRB-SNe (e.g., Cano et al. 2017a, b; Wang et al. 2018; Melandri et al. 2019; Hu et al. 2021; Blanchard et al. 2023; Srinivasaragavan et al. 2024; Gompertz et al. 2024), in which more than one third of the cases have $z < 0.2$. The core-collapse scenario is indirectly supported by the fact that GRBs with $z < 1.2$ are found to be concentrated on the very bright regions of their host galaxies (e.g. Fruchter et al. 2006). On the other hand, the kilonova produced by a merger of a neutron star binary has been confirmed by spectroscopy in only two nearby GRBs, GRB 170817A and GRB 230307A, within a distance of 300Mpc (e.g., Pian et al. 2017; Shappee et al. 2017; Levan et al. 2024). In addition, multi-epoch, high-quality afterglow spectra of bright (usually not very distant) GRBs have been used

to distinguish different scenarios of the interaction between the GRB’s relativistic jet and its environment, and to determine the distance between the GRB and the absorbing material by the variability of the fine-structure lines (e.g., Vreeswijk et al. 2007, 2013; D’Elia et al. 2010, 2014; Kruhler et al. 2013; Hartoog et al. 2013; Wiseman et al. 2017; Pugliese et al. 2024).

Because GRBs usually decay rapidly at their early time, a fast assessment of their distance in prior spectroscopy is quite crucial for mapping out the subsequent observational strategy. This is, however, a hard task for local GRBs. Not as the high- z cases, the afterglow spectral-energy-distribution is useless in the redshift assessment for low- z GRBs because of the lack of the Lyman α break feature (e.g., Wang et al. 2020).

Due to the rapid progress in the time-domain astronomy, a few studies have been recently carried out by aiming at the identification of the host galaxy candidates of extragalactic transients, such as GRBs, fast radio bursts and gravitational wave events, by an approach of probability (e.g., Aggarwal et al. 2021; Ducoin 2023; Demasi et al. 2024). In this paper, by involving the mass of GRB’s host galaxy, we propose a new model that enables us to select local GRB candidates ($z < 0.1$) by a probability that is assessed by a two-dimensional cross-match between GRB afterglows and nearby galaxies with either spectroscopic or photometric redshifts.

The paper is organized as follows. The proposed whole schema of picking-up local GRBs in the SVOM mission¹ are presented in Section 2. Section 3 describes the conception of the proposed model in details. An assessment of the model, along with the used GRB and nearby galaxy samples, are presented in Section 4. Section 5 gives the conclusion and application in the SVOM mission. A Λ CDM cosmological model with parameters $H_0 = 67.4 \text{ km s}^{-1} \text{ Mpc}^{-1}$, $\Omega_m = 0.315$, and $\Omega_\Lambda = 0.685$ (Planck Collaboration et al. 2016) is adopted throughout the paper.

2. SCHEMA OF PICKING-UP LOCAL GRB CANDIDATES IN SVOM

Figure 1 shows the flow chart of picking-up local GRB candidates based on the observations taken by the instruments of the SVOM mission. As shown in the figure, only based on the trigger and follow-up information down-loaded through the VHF network, two independent approaches are designed to select local GRB

candidates. One approach is based on the high-energy prompt emission of a GRB. After excluding the possibility of a high- z GRB candidate ($z > 4$), the other approach is based on a two-dimensional cross-match between a GRB and surrounding nearby galaxies, provided that the GRB has been localized at arcseconds level.

3. THE MODEL

By involving the mass of a galaxy, the probability P_{gal} that a GRB, with a localization at arcseconds level and without a redshift measurement, resides in the galaxy (with z_{gal}) is calculated as

$$P_{\text{gal}} = P_M(M_\star/M_\odot) \times P_A(r_A) \quad (1)$$

where M_\star is the total stellar mass of the galaxy and r_A the linear distance between the GRB and the center of the galaxy if the GRB has z_{gal} . The probability density functions $P_M(M_\star)$ and $P_A(r_A)$ are normalized and described as follows.

There are plenty of studies suggesting that GRB’s host galaxies are biased towards less massive and metallicity poor end (e.g., Vergani et al. 2015; Perley et al. 2016a,b). We determine the $P_M(M_\star/M_\odot)$ from the sample reported in Perley et al. (2016b). With the *Swift* GRB Host Galaxy Legacy Survey, the sample is composed of the host galaxies of 119 bursts. The stellar masses of these galaxies are converted from the corresponding rest-frame near-infrared (NIR) luminosities measured in the deep images taken by *Spitzer Space Telescope*. The distribution of the stellar masses of these GRB host galaxies is shown in the left panel of Figure 2. Modeling the distribution by a Gaussian function

$$P_M(M_\star/M_\odot) = \frac{1}{\sqrt{2\pi}\sigma} e^{-\frac{[\log(M_\star/M_\odot) - \mu]^2}{2\sigma^2}} \quad (2)$$

yields $\mu = 9.73 \pm 0.06$ and $\sigma = 0.64 \pm 0.06$ (the solid blue line overplotted in Figure 2).

We calculate $P_A(r_A)$ by a piecewise exponential distribution

$$P_A(r_A) = \begin{cases} 1, & \text{if } r_A \leq r_e \\ \frac{1}{r_e} e^{-(r_A/r_e)}, & \text{if } r_A > r_e \end{cases} \quad (3)$$

after converting the angular distance θ_A to r_A by $r_A = \theta_A d_A$. $d_A = d_L/(1 + z_{\text{gal}})^2$ is the angular diameter distance, and d_L the luminosity distance. The parameter r_e is the physical size of a galaxy that can be estimated from the stellar mass according to the observed $R - M$ relation given in Shen et al. (2003). Based on 140 000 SDSS galaxies, the authors reported a dependence of

¹ SVOM, launched in 2024, June 22, is a Chinese-French space mission dedicated to the detection and study of GRBs. We refer the readers to Atteia et al. (2022) and the white paper given by Wei et al. (2016) for the details.

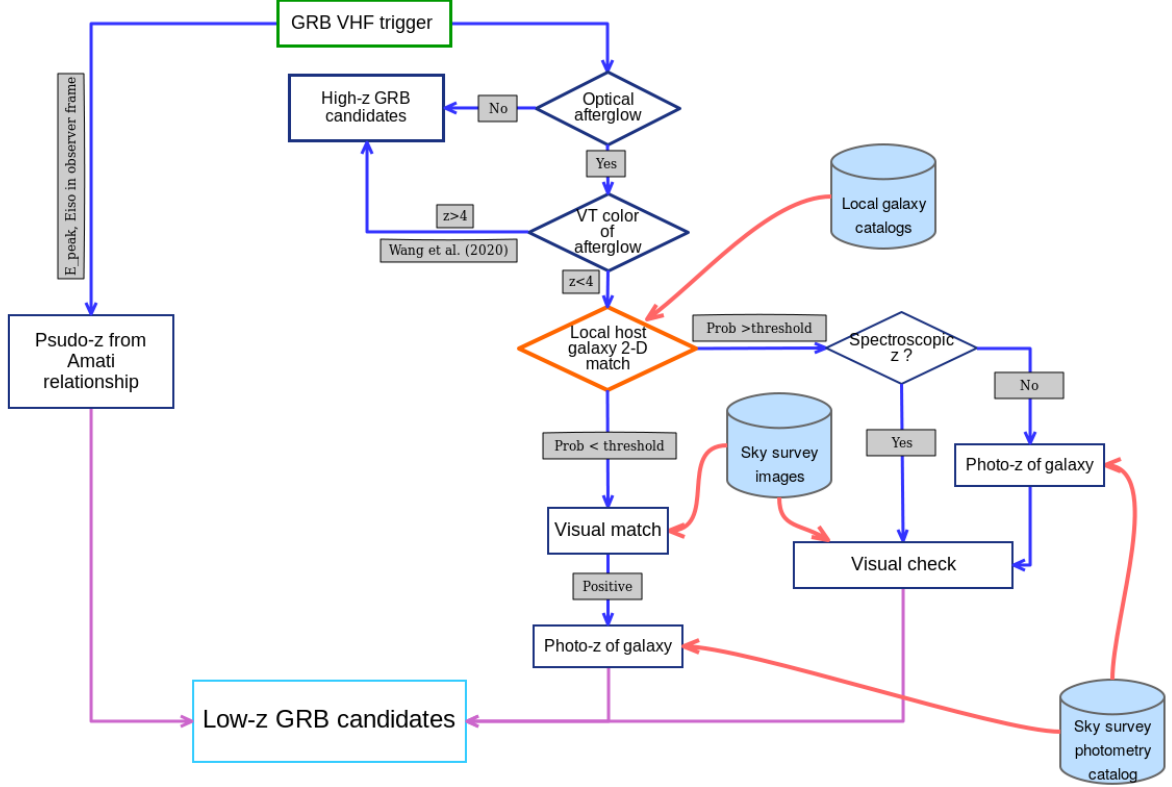


Figure 1. Flow chart of picking-up local GRB candidates in the SVOM mission only by the VHF trigger and follow-ups prior to spectroscopy. The left and right flows depend on the GRB’s prompt emission and the localization of afterglows at arcseconds level, respectively. The data flows and final results are denoted by the blue and magenta arrows. Three external sources, including galaxy catalogs and deep image surveys, are needed to realize the flows. The process related with this paper is emphasized by orange.

R_{50} , the radius enclosing 50% of the Petrosian flux², on luminosity, stellar mass and morphological type. Specifically, the early type galaxies follow:

$$R_{50}^{\text{early}} = 3.47 \times 10^{-5} \left(\frac{M_{\star}}{M_{\odot}} \right)^{0.56} \text{ kpc} \quad (4)$$

and the late type galaxies have

$$R_{50}^{\text{late}} = 0.1 \left(\frac{M_{\star}}{M_{\odot}} \right)^{0.14} \left(1 + \frac{M_{\star}}{M_{\odot}} \right)^{0.39} \text{ kpc} \quad (5)$$

where $M_{\odot} = 3.98 \times 10^{10} M_{\odot}$. Because the morphology is not always available in a galaxy catalog, we adopt $r_e = \max(R_{90}^{\text{early}}, R_{90}^{\text{late}})$ in the current study to avoid an underestimation of the galaxy size, where R_{90} is the radius enclosing 90% of the Petrosian flux. The ratio R_{90}/R_{50} , i.e., the concentration index, is typically ~ 2.3 and ~ 3.3 for an exponential and a de Vaucouleurs profiles, respectively.

² According to the definition given in Petrosian (1976), the Petrosian flux is $\sim 98\%$ and $\sim 80\%$ of the total flux for an exponential and a de Vaucouleurs profiles, respectively.

For a given GRB localized at arcseconds level, each nearby galaxy surrounding the GRB is assigned an association probability calculated by following Eq. (1). The galaxy with the highest association probability P_{max} is then extracted. If $P_{\text{max}} > P_0$, where P_0 is the probability threshold that is determined by the model evaluation and tuning described in the next section, we accept that the galaxy is the most probable host galaxy of the GRB. One should bear in mind that the “acceptation” does not mean the galaxy with $P_{\text{max}} > P_0$ is just the true host, simply because the associated probability is calculated in two-dimension. Due to the absence of radial distance of GRBs, there is likely considerable contamination caused by accident matches between the local galaxies and distant GRBs.

4. MODEL EVALUATION

In this section, our goal is to determine the optimal performance of the proposed model, which is achieved by tuning the probability threshold P_0 based on known nearby galaxy catalogs. Both observed and simulated GRB samples are used in the evaluation.

4.1. The Nearby Galaxy Catalogs

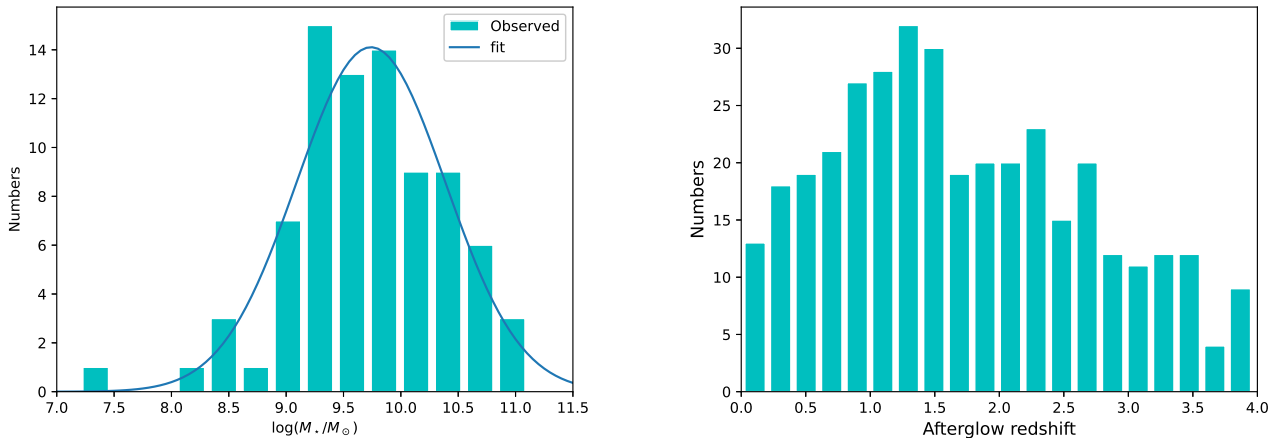


Figure 2. *Left panel:* Distribution of the stellar mass of the host galaxies of a sample of GRBs extracted from Perley et al. (2016b). The best fit Gaussian function with $\mu = 9.73 \pm 0.06$ and $\sigma = 0.64 \pm 0.06$ is overplotted by the blue solid line. *Right panel:* Distribution of the spectroscopic redshifts of a sample of GRBs ($z \leq 4.0$) compiled from the literature.

Two nearby galaxy catalogs are considered in our model evaluation. One is the GLADE+ galaxy catalog³ recently published by Dalya et al. (2022). The catalog is developed for searching for electromagnetic counterparts of advanced gravitational detectors by combining six independent catalogs: the GWGC, 2MPZ, 2MASS XSC, HyerLEAD, WISExSCOPZ and SDSS-DR16 quasar catalogs. It contains ~ 22.5 million galaxies and $\sim 750\,000$ quasars, achieving full completeness in the B -band within a luminosity distance of 47Mpc (corresponding to $z \approx 0.01$). A completeness of $\sim 90\%$ can be achieved at a distance of ~ 500 Mpc ($z \approx 0.1$) when the NIR $W1$ -band is involved. In addition, the catalog provides the total stellar mass estimated from the $W1$ -band brightness.

The other is the NED Local Volume Sample (NED-LVS)⁴ that contains ~ 2 million galaxies with a distance up to 1 Gpc (Cook et al. 2023). Based on the near-IR luminosities, the catalog has a completeness of $\sim 100\%$ at a distance of 30Mpc. The completeness decreases to $\sim 70\%$ up to 300Mpc, and remains $\sim 100\%$ out to ~ 400 Mpc for bright galaxies ($\geq L_*$, L_* is the characteristic luminosity (or “knee”) of the luminosity function).

4.2. Model Evaluation

With the two nearby galaxy catalogs described above, the model presented in Section 3 is evaluated by both observed and simulated GRB samples.

4.2.1. Evaluation from the Observed GRB Sample

A sample of GRBs with spectroscopic redshifts is compiled from literature. An upper limit of $z = 4.0$ is adopted for the sample for two reasons. On the one hand, compared to high- z objects, the Lyman- α break feature is typically weak for objects with $z < 4$ due to the deficient Lyman- α optical depth. On the other hand, there is proven technique for identifying high- z GRB candidates by multi-bands photometry (e.g., Wang et al. 2020). In total, the sample is composed of 365 GRBs with spectroscopic redshifts $z < 4.0$. The right panel of Figure 2 shows the distribution of the redshifts of the GRB sample used in the current study.

With the GRB sample and the nearby galaxy catalogs, we at first calculate the predictions of our model by following the method described in Section 2. For each GRB, the calculation is performed for the galaxies within a circle of $10'^5$. In the GRB sample, there are 343 bursts that have least one galaxy within a circle of $10'$. In the GLADE+ catalog, there are a few galaxies without estimated stellar mass. A default maximum probability of $P_M = 0.17$ is assigned to these galaxies. In both GLADE+ and NED-LVS catalogs, the galaxies without either spectroscopic or photometric redshifts are excluded in the model calculation, after all the fraction of these objects is quite small. The value of P_{\max} is then determined for each GRB by following the method described at the end of Section 3.

In order to extract “true” matches between the 343 GRBs and local galaxies, a revised model in three-

³ <http://glade.elte.hu/>.

⁴ <https://ned.ipac.caltech.edu/NED::LVS/>.

⁵ This large circle is adopted to avoid missing of very nearby and bright galaxies in the calculation. Except that, there is no impact on the final model performance due to the rapid decay of the exponential distribution in Eq (3).

dimensional space is additionally calculated by including the redshifts or distances of the objects listed in the GRB sample. Specifically, for a given GRB, the probability P'_{gal} that a nearby galaxy is associated with it in three-dimensional space can be calculated as

$$P'_{\text{gal}} = P_{\text{M}}(M_{\star}) \times P_{\text{A}}(r_{\text{A}}) \times P_z(\Delta z) \quad (6)$$

where $P_{\text{M}}(M_{\star})$ and $P_{\text{A}}(r_{\text{A}})$ are given in Eqs. (2) and (3), respectively. Similar as $P_{\text{A}}(r_{\text{A}})$, a piecewise exponential distribution

$$P_z(\Delta z) = \begin{cases} 1, & \text{if } \Delta z \leq \Delta z_0 \\ \frac{1}{\Delta z_0} e^{-\Delta z/\Delta z_0}, & \text{if } \Delta z > \Delta z_0 \end{cases} \quad (7)$$

is adopted to calculate the probability in three-dimensional space, where $\Delta z = |z_{\text{GRB}} - z_{\text{gal}}|$ is the redshift difference between the GRB and galaxy. Δz_0 is fixed to be 0.005 in the calculation, which corresponds to a velocity difference of $1,500 \text{ km s}^{-1}$. This velocity difference is large enough to account for the escaping velocity of a few $\times 10^2 \text{ km s}^{-1}$ of a galaxy. For example, the escaping velocity of the Milk Way is between 492 and 594 km s^{-1} .

After calculating the association probability in three-dimensional space, the galaxy with the highest association probability, denoted by P'_{max} , is then identified for each GRB listed in the sample. The probability P'_{max} calculated in three-dimensional space is highly useful for identifying genuine matches between the GRBs and their host galaxies. When the GLADE+ catalog is adopted, the distribution of P'_{max} is in fact found to be concentrated at the extremely small value end. The median and geometric mean of P'_{max} are close to zero for the 343 GRBs. Among the 343 GRBs, there are only nine ones with $P'_{\text{max}} > 1 \times 10^{-4}$. By visually examining the sky images one by one, the truth of the cross-match is validated for 7 out of the 9 GRBs. The details of the validated cross-match of the 7 GRBs is tabulated in Table 1. Figure 3 shows the corresponding sky images.

After identifying of the 7 genuine cross-matches, the performance of the model is assessed by calculating the confusion matrix at various probability threshold P_0 . The matrix is composed of four elements: i.e., the rates of *true* Positive (TP), *false* Positive (FP), *false* Negative (FN) and *true* Negative (TN). Based on the matrix, panels (a) and (b) in Figure 4 shows the dependence of the various assessments, including the Accuracy, Preci-

sion, Recall and F1-score⁶, on the probability threshold P_0 , when the GLADE+ and NED-LVS catalogs are used, respectively. The assessments are calculated by the python/*sklearn* package (Pedregosa et al. 2011).

One can see from both panels that although both Accuracy and Precision increase with the threshold P_0 , there is a consequent decline in the Recall. It means that at a low threshold P_0 despite the fact that local GRBs can be almost completely predicted by the model, there is still significant contamination from accidental cross-matching between distant GRBs and local galaxies. On the contrary, when a high threshold P_0 is adopted, although the contamination is greatly reduced, a substantial number of local GRBs are overlooked in the prediction.

The F1-score is a good assessment providing a balance between Accuracy and Recall, in which the optimal performance of a model can be determined at the peak of F1-score. The determined optimal performance of our model is tabulated in Table 2. Based on the values listed in the table, the model has the optimal performance at the probability threshold $P_0 = 0.05 - 0.09$. At the optimal performance, there are 23-33 true positives in 100 local GRB candidates predicted by the model. At the same time, 4-11 true local GRBs are, however, missed by the model as estimated from the values of Recall.

4.2.2. Evaluation from Simulated GRB Samples

The performance of the proposed model is additionally evaluated by a Monte-Carlo simulation with 1,000 random experiments. Each experiment is implemented

⁶ The parameter of accuracy measures the performance of a model, and is defined as the ratio of total correct instances to the total instances

$$\text{ACC} = \frac{\text{TP} + \text{TN}}{\text{TP} + \text{FP} + \text{FN} + \text{TN}} \quad (8)$$

The parameter of precision measures accuracy of *true* positive predictions, and is defined as the ratio of *true* positive to the total number of positive predictions

$$\text{Precision} = \frac{\text{TP}}{\text{TP} + \text{FP}} \quad (9)$$

The parameter of recall measures the effectiveness of a model in identifying all relevant instances from dataset, and is defined as

$$\text{Recall} = \frac{\text{TP}}{\text{TP} + \text{FN}} \quad (10)$$

The F1-score evaluates the overall performance of a model assessed by the harmonic mean of precision and recall

$$\text{F1} = \frac{2 \cdot \text{Precision} \cdot \text{Recall}}{\text{Precision} + \text{Recall}} \quad (11)$$

The value of F1-score ranges from 0 to 1. It reaches $F1 = 1$ when both Precision and Recall are unity. However, $F1 = 0$ if one of the two parameters is zero. The factor of 2 in the numerator ensures the calculated F1 value are between 0 and 1.

Table 1. The validated seven cross-match between the GRBs and galaxies listed in the GLADE+ catalog.

GRB	Host galaxy	GLADE+ No.	B_{abs} mag	d_L Mpc	M_* $10^{10} M_{\odot}$	r_A "	Δz	P_{max}
(1)	(2)	(3)	(4)	(5)	(6)	(7)	(8)	(9)
060505	614911	-19.7	415	0.5	4.8	0.0012	0.1696
171205A	2MASX J11093966-1235116	1198372	-20.8	175	1.0	6.5	0.0002	0.1570
170817A	NGC 4993	1151336	-19.9	41	2.2	10.0	0.00005	0.1105
190829A	SDSS J025810.28-085719.2	1246359	-21.3	371	4.0	11.6	0.0005	0.0705
980425	ESO184-G82	1265105	-19.3	67	0.1	11.9	0.0063	0.0239
191019A	20916216	-19.7	1206	4.0	0.1	0.0142	0.0047
130702A	14619972	-20.2	843	6.0	7.0	0.0245	0.0004

NOTE—Column (1): GRB name; Column (2): Host galaxy name, if possible; Column (3): The ID of the galaxy in the GLADE+ catalog; Column (4): Absolute magnitude in B -band of the galaxy; Column (5): Distance of the galaxy in unit of Mpc; Column (6): Stellar mass of the galaxy; Column (7): Angular offset (in unit of arcsec) between the GRB’s optical afterglow and the center of the galaxy; Column (8): Redshift difference between the GRB and galaxy; Column (9): The best match probability P_{max} .

Table 2. The best performance of the proposed model.

P_0	Accuracy	Precision	Recall	F-measurement	Galaxy catalog
(1)	(2)	(3)	(4)	(5)	(6)
Observed GRBs					
0.060 – 0.070	0.94	0.23	0.75	0.35	GLADE+
0.051 – 0.089	0.98	0.33	0.75	0.46	NED-LVS
Simulated GRBs					
0.131 ($\beta = 1$)	0.97	0.35	0.35	0.35	GLADE+
0.071 ($\beta = 2$)	0.95	0.20	0.50	0.39	GLADE+

by a random sampling of 100 local GRBs with $z < 0.1$ and of 5 000 GRBs with $z > 0.1$. The ratio of 100:5000 is roughly consistent with the statistics shown in the right panel of Figure 2.

On the one hand, the simulated GRBs with $z > 0.1$ are required to be uniformly distributed on the sky. On the other hand, the celestial positions of the simulated local GRBs are required to follow Eq. (1). Specifically, a sample of local galaxies ($z < 0.1$) following the galaxy mass distribution given in Eq. (2) are at first randomly extracted from a given galaxy catalog. Each extracted galaxy is then paired with an associated GRB, with the linear distance between them is randomly sampled according to the distribution given in Eq. (3).

With the simulated samples, the model is then assessed by following the method used in Section 4.2.1. After an average of the 1,000 random experiments, panel (c) in Figure 4 illustrates the dependence of the various assessments on the probability threshold P_0 , when the GLADE+ catalog is used. One can see from the figure

the F1-score peaks at a large $P_0 = 0.131$, which means the model has the optimal performance with a small Recall= 0.35.

By definition, an assessment based on the F1-score means the Precision and Recall have equal importance. In practice, one, however, would like to reduce the fraction of missed local GRBs as much as possible, provided that the consumption of observational resources remains acceptable. This issue could be addressed by the generalized F-measurement⁷ F_{β} , peaking at different P_0 for different values of β . After determining the peak of F_{β} , a dependence of the probability threshold P_0 on β is shown in Figure 5. Although P_0 decreases with β gener-

7

$$F_{\beta} = \frac{(\beta^2 + 1) \cdot \text{Precision} \cdot \text{Recall}}{\beta^2 \cdot \text{Precision} + \text{Recall}} \quad (12)$$

where β is a parameter. When $\beta = 1$, it reduces to the traditional F1-score. Precision (Recall) has larger weight in the case of $\beta > 1$ ($\beta < 1$).

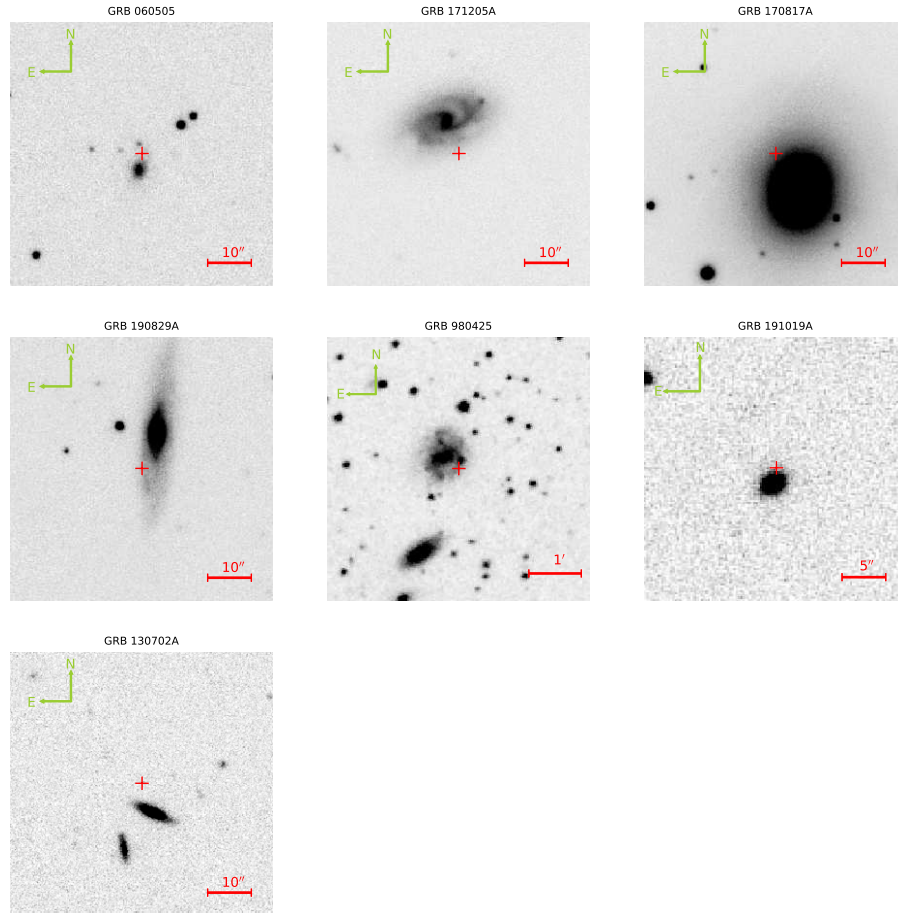


Figure 3. Sky images of the validated seven cross-matches between GRBs and galaxies. All the images obtained in the i -band are extracted from the Pan-STARRS Date Release 1 (Flewelling et al. 2020), except for GRB 980425, whose R -band image is extracted from the DSS2 survey. The size of each image is $1' \times 1'$, except for the cases of GRB 980425 and GRB 191019A whose images have a size of $5' \times 5'$ and $30'' \times 30''$ respectively. In each panel, the position of the GRB’s afterglow is at the center and marked by a red cross. The north and east are at top and left, respectively.

ally, two steps can be learned from the figure. One step occurs at $\beta \sim 1$, and the other at $\beta \sim 2$. Again, Table 2 lists the corresponding values of the assessments in both $\beta = 1$ and $\beta = 2$ cases. In the case of $\beta = 2$, the optimal performance of the model has an increased Recall= 0.5 and reduced Precision= 0.20, which means a half of the true local GRBs would be missed by the model with a probability threshold $P_0 = 0.07$.

4.3. Comparison with Other Algorithms

The results returned from the model proposed in this study are compared to two other algorithms recently re-

ported in literature, by using the same observed GRB sample (i.e., the right panel in Figure 2). On the one hand, by involving the ALLWISE catalog (Cutri et al. 2013), Pan-STARRS catalog (Chambers et al. 2016), Hubble Source catalog (Whitmore et al. 2016) and GLADE catalog (Dalya et al. 2018), only one association between GRB 170817A and NGC 4993 has been claimed by the Galclaim tool⁸ (Ducoin et al. 2023). The tool aims at identifying an association between a

⁸ <https://github.com/jgducoin/galclaim>.

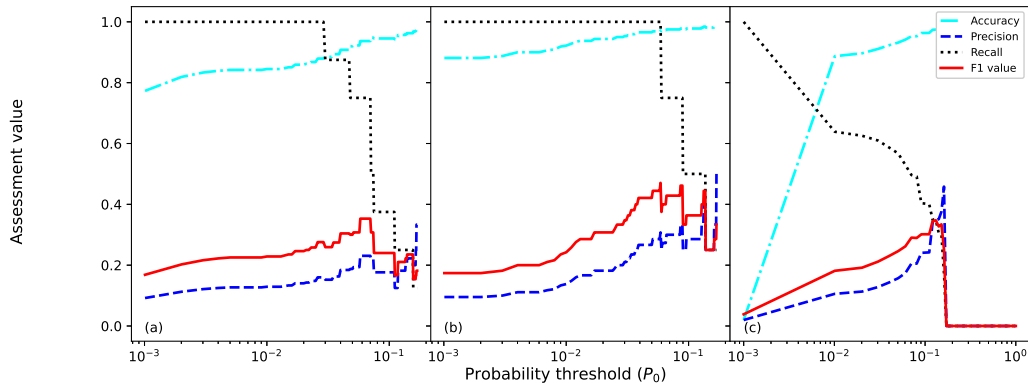


Figure 4. *Panel (a):* Various assessments (see footnote 6 for the definitions) of the model plotted against the probability threshold P_0 when the observed GRB sample and the GLADE+ catalog are used. The optimal performance of the model can be determined by the peak of F1-score. *Panel (b):* the same as panel (a) but for the case in which the NED-LVS catalog is used. *Panel (c):* the same as panel (a) but for the simulated GRB samples.

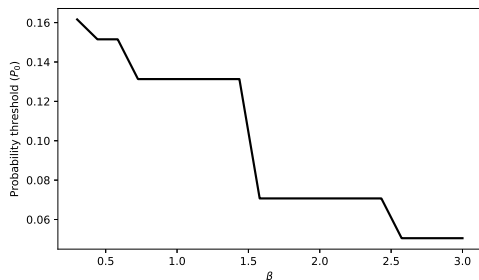


Figure 5. Probability threshold (P_0) determined by the peak of F-measurement (see footnote 7) plotted against β , when the model is assessed by the simulated GRB samples and the GLADE+ catalog.

transient and corresponding host galaxy by the probability of chance alignment.

On the other hand, as an additional comparison, we run the tool of `astropath`⁹ (Aggarwal et al. 2021) based on the GLADE+ catalog. The tool is designed to predict an association of a FRB and its host galaxy by posterior probability calculated based on the rule of Bayes. With the same observed GRB sample used in the current study, seven associations with a posterior probability > 0.9 are in total predicted by the tool. There is, however, only one true association (i.e., GRB 060505) among the seven events after a visual examination one by one. The other 6 predicted associations are easily identified as being incorrect, because of the significant redshift difference between the observed afterglows and predicted host galaxies.

⁹ <https://github.com/FRBs/astropath>.

5. CONCLUSION AND APPLICATION

By involving the masses and physical sizes of GRB’s host galaxies, a model based on two-dimensional cross-match probability is developed in this paper to identify local GRB candidates as soon as possible after the triggers and before spectroscopy. The model is developed in the python 3.10 environment. The packages of NumPy, SciPy (Virtanen et al. 2020), and scikit-learn module (Pedregosa et al. 2011) are required for running the model. With the GLADE+ and NED-LVS galaxy catalogs with a completeness of at least $\sim 70\%$ up to $\sim 300\text{Mpc}$, the optimal performance of the model has a Precision of 0.23 – 0.33 and a Recall of 0.75 determined by the observed GRB sample. The optimal performance has a reduced Recall of 0.35 – 0.50 when the simulated GRB samples are adopted.

Figure 6 shows an example of implementation of the model in terms of a developed web service. In addition to the predicted association probability, the tool allows users to examine the predicted GRB-galaxy match visually, and will be integrated into the SVOM Science User Support System¹⁰ to help the SVOM burst advocates and GRB scientists to identify candidates of high-value source and to reasonably allocate observational resources, especially spectroscopy, as soon as possible, which is crucial for enhancing the scientific returns of the SVOM mission.

Due to the incorporation of galaxy mass (as well as its physical size) into the model, the redshifts (either spectroscopic or photometric) or distances of galaxies are necessary in the model prediction. This is, however,

¹⁰ <https://www.svom.cn/suss/#/home>

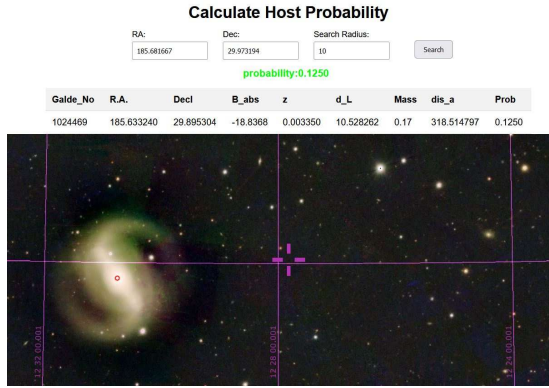


Figure 6. Implementation of the model of identifying nearby GRBs by their most probable host galaxies. GRB 241218A with a *Swift*/XRT enhanced localization with an accuracy of arcsec (Beardmore et al. 2024) is used as an example. The calculated possibility of 0.1250 shown in green means the value is larger than the probability threshold P_0 of our model. The positions of the GRB and the galaxy with the highest cross-match probability are marked by the magenta cross and red circle, respectively.

a serious problem for the faint galaxies that either lack a redshift measurement in existing catalogs or are entirely excluded from the existing catalogs. This issue could be

alleviated by estimating photometric redshifts (photo- z) by fitting their spectral energy distributions if the multi-wavelength photometry is available. This approach is essential for a visual examination when a deep survey (e.g., DESI) is used. The photo- z estimation based on public code (e.g., *Hyperz*, Bolzonella et al. 2011) will be integrated into the web service in the next step.

ACKNOWLEDGMENTS

The authors are thankful for support from the National Key R&D Program of China (grant No. 2024YFA1611700). This study is supported by the Strategic Pioneer Program on Space Science, Chinese Academy of Sciences, grants XDB0550401. JW is supported by the National Natural Science Foundation of China (Grants No. 12173009). EWL is supported by the National Science Foundation of China (grant No. 12133003) and the Guangxi Talent Program (“Highland of Innovation Talents”).

Software: MATPLOTLIB (Hunter 2007), PYTHON/sklearn (Pedregosa et al. 2011)

REFERENCES

- Aggarwal, K., Budavári, T., Deller, A. T., et al. 2021, *ApJ*, 911, 95
- Atteia, J.-L., Cordier, B., & Wei, J. 2022, *International Journal of Modern Physics D*, 31, 2230008
- Beardmore, A. P., Evans, P. A., Goad, M. R., et al. 2024, *GCN CIRCULAR*, 38604
- Berger, E. 2014, *ARA&A*, 52, 43
- Blanchard, P. K., Villar, V. A., Chornock, R., et al. 2023, *GRB Coordinates Network, Circular Service*, No. 33676
- Bolzonella, M., Miralles, J.-M., & Pelló, R. 2011, *Astrophysics Source Code Library*
- Cano, Z., Izzo, L., de Ugarte Postigo, A., et al. 2017a, *A&A*, 605, A107
- Cano, Z., Wang, S.-Q., Dai, Z.-G., et al. 2017b, *Advances in Astronomy*, 2017, 8929054
- Cook, D. O., Mazzarella, J. M., Helou, G., et al. 2023, *ApJS*, 268, 14
- Chambers, K. C., Magnier, E. A., Metcalfe, N., et al. 2016, *arXiv:1612.05560*
- Cucchiara, A., Levan, A. J., Fox, D. B., et al. 2011, *ApJ*, 736, 7
- Cutri, R. M., Wright, E. L., Conrow, T., et al. 2013, *Explanatory Supplement to the AllWISE Data Release Products*, by R. M. Cutri et al.
- Dály, G., Díaz, R., Bouchet, F. R., et al. 2022, *MNRAS*, 514, 1403
- Dály, G., Galgóczi, G., Dobos, L., et al. 2018, *MNRAS*, 479, 2374
- D’Elia, V., Fynbo, J. P. U., Goldoni, P., et al. 2014, *A&A*, 564, A38
- D’Elia, V., Fiore, F., Goldoni, P., et al. 2010, *MNRAS*, 401, 385
- Demasi, G., Capurri, G., Ricciardone, A., et al. 2024, *arXiv:2407.13695*.
- Ducoin, J.-G. 2023, *SoftwareX*, 24, 101582
- Flewelling, H. A., Magnier, E. A., Chambers, K. C., et al. 2020, *ApJS*, 251, 7
- Fruchter, A. S., Levan, A. J., Strolger, L., et al. 2006, *Nature*, 441, 463
- Gompertz, B. P., Levan, A. J., Malesani, D. B., et al. 2024, *GRB Coordinates Network, Circular Service*, No. 37867
- Greiner, J., Kruhler, T., Fynbo, J. P. U., et al. 2009, *ApJ*, 693, 1610
- Hjorth, J., & Bloom, J. S. 2012, *The Gamma-Ray Burst-Supernova Connection*, 9 (Cambridge: Cambridge Univ. Press), 169
- Hartoog, O. E., Wiersema, K., Vreeswijk, P. M., et al. 2013, *MNRAS*, 430, 2739

- Hu, Y.-D., Castro-Tirado, A. J., Kumar, A., et al. 2021, *A&A*, 646, A50
- Krühler, T., Ledoux, C., Fynbo, J. P. U., et al. 2013, *A&A*, 557, A18
- Lamb, D. Q. & Reichart, D. E. 2000, *ApJ*, 536, 1
- Levan, A. J., Gompertz, B. P., Salafia, O. S., et al. 2024, *Nature*, 626, 737
- Melandri, A., Bernardini, M. G., D'Avanzo, P., et al. 2015, *A&A*, 581, A86
- Melandri, A., Malesani, D. B., Izzo, L., et al. 2019, *MNRAS*, 490, 5366
- Pedregosa, F., Varoquaux, G., Gramfort, A., et al. 2011, *JMLR*, 12, 2825
- Perley, D. A., Krühler, T., Schulze, S., et al. 2016a, *ApJ*, 817, 7
- Petrosian, V. 1976, *ApJL*, 210, L53
- Pian, E., D'Avanzo, P., Benetti, S., et al. 2017, *Nature*, 551, 67
- Planck Collaboration, Ade, P. A. R., Aghanim, N., et al. 2016, *A&A*, 594, A13
- Shappee, B. J., Simon, J. D., Drout, M. R., et al. 2017, *Science*, 358, 1574
- Shen, S., Mo, H. J., White, S. D. M., et al. 2003, *MNRAS*, 343, 978
- Srinivasaragavan, G. P., Swain, V., O'Connor, B., et al. 2024, *ApJL*, 960, L18
- Tagliaferri, G., Antonelli, L. A., Chincarini, G., et al. 2005, *A&A*, 443, L1
- Tanvir, N. R., Fox, D. B., Levan, A. J., et al. 2009, *Nature*, 461, 1254
- Vergani, S. D., Salvaterra, R., Japelj, J., et al. 2015, *A&A*, 581, A102
- Virtanen, P., Gommers, R., Oliphant, T. E., et al. 2020, *Nature Methods*, 17, 261
- Vreeswijk, P. M., Ledoux, C., Raassen, A. J. J., et al. 2013, *A&A*, 549, A22
- Vreeswijk, P. M., Ledoux, C., Smette, A., et al. 2007, *A&A*, 468, 83
- Wang, J., Zhu, Z. P., Xu, D., et al. 2018, *ApJ*, 867, 147
- Wang, J., Qiu, Y. L., & Wei, J. Y. 2020, *RAA*, 20, 124
- Wei, J. Y., Cordier, B., Antier, S., et al. 2016, [arXiv:astro-ph/1610.0689](https://arxiv.org/abs/1610.0689)
- Whitmore, B. C., Allam, S. S., Budavári, T., et al. 2016, *AJ*, 151, 134
- Wiseman, P., Perley, D. A., Schady, P., et al. 2017, *A&A*, 607, A107
- Woosley, S. E., & Bloom, J. S. 2006, *ARA&A*, 44, 507